A fast local level set adjoint state method for first arrival transmission traveltime tomography with discontinuous slowness

Wenbin Li* Shingyu Leung†

April 30, 2013

Abstract

We propose a numerical algorithm for solving first arrival transmission traveltime tomography problems where the underlying slowness is piecewise continuous. The idea is based upon our previously efficient approach for smooth slowness inversion [28] using the fast sweeping method and the adjoint state method. In this work, we further incorporate the level set method to implicitly represent the discontinuity in the velocity. One main advantage of such implicit representation is that there is no assumption on the number of disjoint components in the inverted structure. The evolution of the level set function will naturally take care of the change in the topology. Like in the previous work, the gradient of the mismatch functional is derived using the adjoint state method. The forward problem and the adjoint equation are efficiently solved by the fast sweeping method. To further improve the computational efficiency, we also propose a local level set method so that most computer power of updating the level set evolution is spent near the discontinuity in the slowness. Numerical results will be given to demonstrate the robustness of the algorithm.

1 Introduction

Traveltime tomography is an important class of inverse problems which tries to determine the internal velocity or slowness of a medium by the traveltime of high frequency waves between point sources and receivers [3, 43, 44, 32, 54, 55, 57, 33, 27, 29]. In this paper, we concentrate on the transmission traveltime tomography problem using only first arrival information. Traditional solution methods rely on ray tracing techniques based on the Fermat's principle. For example, [4] proposed an algorithm to determine the first arrival traveltime in a ray tracing framework. Since then, many extensions to the inverse problem have been developed in the geophysics community more or less depending on a similar idea [7]. In differential geometry, using the first arrival traveltime tomography is referred to the boundary rigidity problem in Riemannian geometry. Significant amount of progress has been made recently on the theoretical advances [47, 48, 49, 50, 51, 52]. Based on these recent theories, [10, 11, 12] have developed Lagrangian ray tracing based algorithms to recover the Riemannian manifolds in terms of the refraction index.

However, one major drawback of these Lagrangian approaches to first arrival transmission traveltime tomography is that one has to develop a natural numerical approach to figure out the first arrival ray from multiple arrivals [41]. Also, since the curved rays are traveled in the inhomogeneous medium, there could be shadow regions between point sources and receivers [56, 1, 2].

In [28], we have proposed a simple partial differential equation (PDE) based approach so one can avoid using the ray tracing method. For the forward problem, we model the first arrival traveltimes from point sources by using the eikonal equation. The viscosity solution of the Hamilton-Jacobi equation guarantees the first arrival at all receiver locations from a single point source [14]. The fundamental idea in our previous work is to minimize a mismatch functional where the gradient of the energy is efficiently determined by solving an adjoint state equation. To stabilize the gradient flow, we have further regularized the descent direction by a Tikhonov method which relies on the L^2 norm. Therefore one would expect that the approach will lead to a continuous inverted velocity. We refer interested readers to [16] for some theoretical analysis of the approach. Numerically, the Hamilton-Jacobi equation in the

*Department of Mathematics, the Hong Kong University of Science and Technology, Clear Water Bay, Hong Kong. Email: **lwb@ust.hk**

†Department of Mathematics, the Hong Kong University of Science and Technology, Clear Water Bay, Hong Kong. Email: **masyleung@ust.hk**

forward problem can be efficiently solved using the Fast Sweeping methods [53, 25, 58, 39, 40]. Concerning the adjoint variable, we have also proposed in [28] an efficient sweeping-like iterative approach. These tools have lead to a computationally very efficient numerical algorithm for the inverse problem. A similar inverse problem has recently been considered in [26] where the solution is determined on a triangular mesh using the Fast Marching method.

In practice, however, most important velocity models are discontinuous in the crust and lithosphere. The above approach will not work well since the regularity in the solution is too strong for the application. The above Tikhonov regularity requires that the inverted solution to be continuous in the whole domain. In this paper, we propose to extend the previous work [28] on first arrival transmission traveltime tomography by restricting the inverted slowness in the class of piecewise continuous functions. The inverse problem we are solving is the following: given first arrival measurements on the boundary, we determine a piecewise continuous slowness and also the location of the discontinuity. In particular, the discontinuity in the velocity is represented implicitly using the level set method [35, 45, 34]. One main advantage of such implicit representation is that there is no assumption on the connectivity of the discontinuities in the inverted structure. There could be many disjointed components in the slowness. We can start the initial iteration with a guess of one single discontinuous component. The evolution of the level set function will naturally take care of the change in the topology.

Level set method can be applied to solve a wide range of inverse problems. For example, the level set method has first been used in [42] for inverse problems involving obstacles. Later on, there are many efforts to analyze this method and extend such idea to a variety of inverse problems, including shape-optimization, optimal design and inverse gravimetry; see for example [30, 5, 6, 9, 18, 21, 22] and references therein.

In seismic applications, it is worth noticing an interesting recent work in [59] which considers also transmission traveltime tomography with discontinuous slowness. In the article, the authors have also developed a level set formulation based on our previous work on the adjoint state method [28]. We both incorporate the level set method to implicitly represent the discontinuity in the velocity. However, [59] further simplifies the inverse problem by assuming that both the inside and the outside slowness are **known**, which essentially reduces the inverse problem to a shape optimization problem.

A related, yet different, inverse problem is the reflection traveltime tomography which concentrates on the wave reflected by the discontinuity in the slowness [17, 13, 12, 20]. For example, an interesting recent paper [20] has studied a joint transmission and reflection traveltime tomography problem. Like our works, the forward problem is modeled by the eikonal equation and is solved numerically using the Fast Sweeping method, while the variational derivative is also computed by the adjoint state technique. However, the location for the discontinuity in the model is assumed to be **known** and one inverts the velocity only within certain sub-domain where the velocity is assumed to be continuous. The location of the discontinuity is not a part of their inverse problem.

The rest of the paper is organized as follows. We will first briefly describe the forward problem mathematically in Section 2. In Section 3 we will propose the variational formulation based on the level set method for the inverse problem. A simplified model will be studied in Section 4. Details in numerical implementation will be given in Section 5. To demonstrate the effectiveness of the model, we will study various test examples in Section 6. Finally in Section 7, we will discuss some limitations of the proposed method.

2 Background

The eikonal equation is a non-linear first order Hamilton-Jacobi which describes the behavior of high frequency wave:

$$|\nabla T(\mathbf{x})| = S(\mathbf{x}), \qquad \mathbf{x} \in \Omega \setminus P \tag{2.1}$$

$$T(\mathbf{x}_s) = 0, \qquad \mathbf{x}_s = P \tag{2.2}$$

where $T(\mathbf{x})$ is the traveltime of the wave from point source $\mathbf{x}_s$ to $\mathbf{x}$, $S(\mathbf{x})$ is the slowness of the media, P is the set of point source locations.

For continuous slowness $S(\mathbf{x}) \in C(\Omega)$, the equation admits the well-known viscosity solution [14] and such solution corresponds to the first-arrival traveltime. For discontinuous slowness, [36] has introduced the concept of extended viscosity solution to carefully study the well-poseness of the equation. Roughly speaking, when $S(\mathbf{x})$ is piecewise Lipschitz continuous, the eikonal equation admits the extended viscosity solution which is Lipschitz continuous, and such solution corresponds also to the first-arrival traveltime.

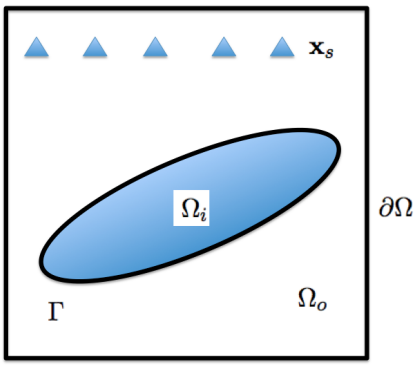

Figure 1: Problem statement.

Moreover, any finite difference scheme that is monotonic in $S(\mathbf{x})$ and converges to the viscosity solution for continuous $S(\mathbf{x})$ must also converge to the extended viscosity solution for discontinuous $S(\mathbf{x})$ [24]. Another analysis for Hamilton-Jacobi equations with discontinuities can be found in [15].

Then the related inverse problem reads as follows: given the extended viscosity solution $T(\mathbf{x})$ on the boundary $\partial\Omega$ and the location of point sources $\mathbf{x}_s \in \Omega$, we want to invert for the slowness $S(\mathbf{x})$ in Ω. Here $T(\mathbf{x})|_{\partial\Omega}$ is the first arrival traveltime measured on the boundary and $S(\mathbf{x})$ in Ω reveals the structure of the media. The set up is shown in Figure 1. In this work we are interested in media with piecewise continuous structure, such as an oil field where one region is oil and the other is rock. Then the slowness $S(\mathbf{x})$ can be expressed as: $S(\mathbf{x}) = S_i(\mathbf{x})$, $\mathbf{x} \in \Omega_i$; $S(\mathbf{x}) = S_o(\mathbf{x})$, $\mathbf{x} \in \Omega_o$, where $\Omega_o \cup \Omega_i = \Omega$, $S_i(\mathbf{x})$ and $S_o(\mathbf{x})$ are continuous and bounded functions.

3 The level set adjoint state method

In this section, we will briefly introduce the level set method and then explain how we incorporate it with the adjoint state method for the inverse problem in Section 3.1. We will then discuss the general case where the target slowness is piecewise continuous in Section 3.2. Method to deal with multiple point sources and regularization techniques will be given in Sections 3.3 and 3.4, respectively.

3.1 A level set representation and a variational formulation

Level set method [35] is a powerful numerical tool for modeling the evolution of a dynamic interface. The idea is to represent the interface implicitly by the zero level set of a level set function, with the corresponding motion of the interface governed by a corresponding partial differential equation (PDE). In this section, we will only briefly introduce necessary concepts for the work and we refer any interested reader for a more complete description in [45, 34].

To implicitly represent the discontinuity in the slowness, we introduce a level set function $\phi(\mathbf{x})$ with the discontinuity denoted by its zero level set $\phi^{-1}(0)$, i.e. $\Gamma = \phi^{-1}(0)$. Further, for the reason of numerical stability, we require $\phi(\mathbf{x})$ to be a signed distance function such that

$$\phi(\mathbf{x}) = \begin{cases} \text{dist}(\mathbf{x},\Gamma) \ , \ \mathbf{x} \in \Omega_o \\ -\text{dist}(\mathbf{x},\Gamma) \ , \ \mathbf{x} \in \Omega_i \end{cases}, \quad \Gamma = \bar{\Omega}_o \cap \bar{\Omega}_i ,$$

where $\text{dist}(\mathbf{x},\Gamma)$ is the shortest distance from $\mathbf{x} \in \Omega$ to the location of discontinuity Γ. With this level set function, the discontinuous slowness of the media can be represented implicitly by

$$S(\mathbf{x}) = S_o(\mathbf{x}) \cdot H(\phi(\mathbf{x})) + S_i(\mathbf{x}) \cdot [1 - H(\phi(\mathbf{x}))] , \tag{3.3}$$

where $H : \mathbb{R} \to \mathbb{R}$ is the Heaviside function

$$H(x) = \begin{cases} 1 \ , \ x > 0 \\ 0 \ , \ x < 0 \end{cases} .$$

In equation (3.3), the discontinuous slowness $S(\mathbf{x})$ is constructed by three continuous functions: $S_o(\mathbf{x})$, $S_i(\mathbf{x}) \in C(\bar{\Omega})$, and the signed distance level set function $\phi(\mathbf{x})$. In practice, a reasonable assumption is that

the physical property of the outer region is known such that $S_o(\mathbf{x})$ is given. Then the inverse problem is to invert both the slowness of the inner region $S_i(\mathbf{x})$ and the level set function $\phi(\mathbf{x})$ using the first arrival measurements given on the boundary $\partial\Omega$. Note that the function $S_i(\mathbf{x})$ is defined everywhere in Ω even though it is physically meaningful only in Ω_i.

Based on the techniques we developed in [28, 29], we propose to solve the inverse problem by minimizing the following mismatching functional given by

$$E(S)=E(\phi,S_i)=\frac{1}{2}\int_{\partial\Omega}|T(\phi,S_i)-T^*|^2\,\mathrm{d}s,$$

where $T^*|_{\partial\Omega}$ is the first arrival traveltime measured by sensors located along the boundary $\partial\Omega$, and $T(\phi,S_i)|_{\partial\Omega}$ is the viscosity solution computed by solving (2.1) with one single point source (2.2) for given $\phi(\mathbf{x})$ and $S_i(\mathbf{x})$. Following the same argument in [28, 29], this energy $E(S)$ describes the L^2-difference between the exact traveltime T^* and the computed traveltime T on the boundary.

To minimize this functional with respect to ϕ and S_i, we use the method of gradient descent. In the following subsection, we give a rigorous mathematical derivation of the derivatives using the adjoint state method.

3.2 Adjoint state method for the gradient

Following the method of gradient descent, we perturb the initial level set function ϕ by a small amount $\epsilon\tilde{\phi}$ and the function S_i by $\epsilon\tilde{S}$. The corresponding perturbation on $S(\phi,S_i)$ can be calculated by (3.3),

$$\begin{aligned}&S(\phi+\epsilon\tilde{\phi},S_i+\epsilon\tilde{S})-S(\phi,S_i)\\=&(S_o(\mathbf{x})-S_i(\mathbf{x}))\cdot(H(\phi+\epsilon\tilde{\phi})-H(\phi))\\&+\epsilon\tilde{S}\cdot(1-H(\phi+\epsilon\tilde{\phi})).\end{aligned}$$

To understand this perturbation, we regularize the Heaviside function using a smoothed version by introducing a small parameter τ $(0<\tau<1)$,

$$H_\tau(\phi)=\frac{1}{2}\left(\tanh\frac{\phi}{\tau}+1\right).$$

Therefore, we have

$$S(\mathbf{x})=S_o(\mathbf{x})\cdot H_\tau(\phi(\mathbf{x}))+S_i(\mathbf{x})\cdot[1-H_\tau(\phi(\mathbf{x}))],\tag{3.4}$$

and so

$$\begin{aligned}&S(\phi+\epsilon\tilde{\phi},S_i+\epsilon\tilde{S})-S(\phi,S_i)\\=&(S_o(\mathbf{x})-S_i(\mathbf{x}))\cdot(H_\tau(\phi+\epsilon\tilde{\phi})-H_\tau(\phi))\\&+\epsilon\tilde{S}\cdot(1-H_\tau(\phi+\epsilon\tilde{\phi})).\end{aligned}\tag{3.5}$$

To get the perturbation in the Heaviside function, we have

$$\begin{aligned}&H_\tau(\phi+\epsilon\tilde{\phi})-H_\tau(\phi)\\=&H'_\tau(\phi)\cdot\epsilon\tilde{\phi}+\frac{H''_\tau(\xi)}{2!}(\epsilon\tilde{\phi})^2\\=&\epsilon\tilde{\phi}\cdot\frac{1}{2\tau\cdot\cosh^2\frac{\phi}{\tau}}-\epsilon^2\tilde{\phi}^2\cdot\frac{\tanh\frac{\xi}{\tau}}{2\tau^2\cdot\cosh^2\frac{\xi}{\tau}}\end{aligned}\tag{3.6}$$

for some $\xi\in(\phi,\ \phi+\epsilon\tilde{\phi})$ and $\xi=O(\phi)$ with the notation $f=O(g)$ means $\exists\ C>0$, such that $|f|\le C|g|$. Consider $\phi=O(\tau^\alpha)$, substitute it into (3.6) and note $\xi=O(\phi)$, we get

$$\begin{aligned}&H_\tau(\phi+\epsilon\tilde{\phi})-H_\tau(\phi)\\=&\frac{\epsilon}{2\tau\cdot\cosh^2(O(\tau^{\alpha-1}))}\cdot\tilde{\phi}-\frac{\epsilon^2\cdot\tanh\left(O\left(\tau^{\alpha-1}\right)\right)}{2\tau^2\cdot\cosh^2(O(\tau^{\alpha-1}))}\cdot\tilde{\phi}^2\\=&\begin{cases}\frac{\epsilon}{\tau}\cdot O(1)-\frac{\epsilon^2}{\tau^2}\cdot O(1) & ,\text{ when }\alpha\ge1,\\ O(\epsilon) & ,\text{ when }\alpha<1.\end{cases}\end{aligned}\tag{3.7}$$

The estimate of the order is in the sense of $\tau\to 0$. Note that $\phi=O(\tau^\alpha)$ where $\alpha\geq 1$ only near the interface Γ. In the limit as τ tends to 0, such region is of zero measure. Also to control the magnitude of the perturbation, we choose $\epsilon\leq\tau$ so that $\frac{\epsilon}{\tau}=O(1)$ and $\frac{\epsilon^2}{\tau^2}=O(1)$.

As a result, (3.7) gives

$$H_\tau(\phi+\epsilon\tilde{\phi})-H_\tau(\phi)=\begin{cases} O(1),\ \phi=O(\tau^\alpha),\ \alpha\geq 1 \\ O(\epsilon),\ \phi=O(\tau^\alpha),\ \alpha<1 \end{cases}. \tag{3.8}$$

Substituting (3.8) into (3.5), we get the same result for the perturbation on $S(\phi,S_i)$,

$$S(\phi+\epsilon\tilde{\phi},S_i+\epsilon\tilde{S})-S(\phi,S_i)=\begin{cases} O(1),\ \phi=O(\tau^\alpha),\ \alpha\geq 1 \\ O(\epsilon),\ \phi=O(\tau^\alpha),\ \alpha<1 \end{cases}.$$

Now, the perturbation in $T(\mathbf{x})$ depends on the accumulation of the slowness along the ray reaching $\mathbf{x}$, we look at

$$T(\mathbf{x})=\int_0^L S(s)ds,$$

for the arc-length parametrization of the ray s from the point source to the point $\mathbf{x}$. And so,

$$T(\mathbf{x})=\int_{[0,L]\cap\{\phi=O(\tau^\alpha),\alpha\geq 1\}} S(s)ds+\int_{[0,L]\cap\{\phi=O(\tau^\alpha),\alpha<1\}} S(s)ds.$$

Since the measure of the set $\{\phi=O(\tau^\alpha),\alpha\geq 1\}$ is $O(\tau)=O(\epsilon)$, we expect that the corresponding perturbation on the traveltime T is of $O(\epsilon)$ and we denote it by $T(\phi+\epsilon\tilde{\phi},S_i+\epsilon\tilde{S})-T(\phi,S_i)=\epsilon\tilde{T}$.

Using the eikonal equation (2.1), these perturbations $\tilde{\phi}$, $\tilde{S}$ and $\tilde{T}$ are related by

$$2\epsilon\cdot\nabla T\cdot\nabla\tilde{T}+O(\epsilon^2)=S^2(\phi+\epsilon\tilde{\phi},S_i+\epsilon\tilde{S})-S^2(\phi,S_i). \tag{3.9}$$

Now, except the region $\{\phi=O(\tau^\alpha),\alpha\geq 1\}$ which has measure zero as τ tends to 0, the following order estimates are valid almost everywhere in the domain. From (3.5) and (3.6),

$$\begin{aligned} &S(\phi+\epsilon\tilde{\phi},S_i+\epsilon\tilde{S}) \\ &=S(\phi,S_i)+\epsilon\tilde{\phi}\cdot\frac{S_o-S_i}{2\tau\cdot\cosh^2\frac{\phi}{\tau}} \\ &\quad+\epsilon\tilde{S}\cdot(1-H_\tau(\phi))+O(\epsilon^2). \end{aligned} \tag{3.10}$$

Substituting (3.10) into (3.9), we obtain

$$\begin{aligned} &2\epsilon\cdot\nabla T\cdot\nabla\tilde{T}+O(\epsilon^2) \\ &=\epsilon\tilde{\phi}\cdot\frac{(S_o-S_i)\cdot S(\phi,S_i)}{\tau\cdot\cosh^2\frac{\phi}{\tau}} \\ &\quad+\epsilon\tilde{S}\cdot 2(1-H_\tau(\phi))\cdot S(\phi,S_i)+O(\epsilon^2). \end{aligned} \tag{3.11}$$

To simplify the notation, we denote

$$A(\phi,S_i)=\frac{(S_o-S_i)\cdot S(\phi,S_i)}{2\tau\cdot\cosh^2\frac{\phi}{\tau}}, \tag{3.12}$$

$$B(\phi,S_i)=(1-H_\tau(\phi))\cdot S(\phi,S_i). \tag{3.13}$$

Now, we match $O(\epsilon)$ terms in (3.11) and get

$$\tilde{\phi}\cdot A(\phi,S_i)+\tilde{S}\cdot B(\phi,S_i)-\nabla T\cdot\nabla\tilde{T}=0. \tag{3.14}$$

Following the adjoint state method [8, 38, 28], we multiply (3.14) by $\epsilon\lambda$, integrate it over Ω and add to

the change of mismatching energy, we get

$$\begin{aligned}
&(\delta E)/\epsilon \\
&= [E(\phi+\epsilon\tilde{\phi}, S_i+\epsilon\tilde{S}) - E(\phi, S_i)]/\epsilon \\
&= \int_{\partial\Omega} \tilde{T}\cdot(T(\phi,S_i)-T^*)\,\mathrm{d}s + O(\epsilon) \\
&= \int_{\partial\Omega} \tilde{T}\cdot(T(\phi,S_i)-T^*)\,\mathrm{d}s + O(\epsilon) + \\
&\quad \int_{\Omega} \lambda\cdot(\tilde{\phi}\cdot A(\phi,S_i)+\tilde{S}\cdot B(\phi,S_i)-\nabla T\cdot\nabla\tilde{T})\,\mathrm{d}\mathbf{x} \\
&= \int_{\Omega} \left(\lambda A(\phi,S_i)\cdot\tilde{\phi}+\lambda B(\phi,S_i)\cdot\tilde{S}+\mathrm{div}(\lambda\nabla T)\cdot\tilde{T}\right)\mathrm{d}\mathbf{x} \\
&\quad + \int_{\partial\Omega}\left(T-T^*-\lambda\frac{\partial T}{\partial n}\right)\cdot\tilde{T}\,\mathrm{d}s + O(\epsilon),
\end{aligned} \tag{3.15}$$

where n denotes the unit outward normal of $\partial\Omega$. Notice once again that one might worry about the region $\{\phi = O(\tau^\alpha), \alpha \geq 1\}$ in the analysis (3.10-3.11), the measure of the set is 0 as τ tends to 0. Therefore, it has no effect on the integral (3.15). Finally, if the adjoint variable λ satisfies

$$\begin{aligned}
-\mathrm{div}(\lambda\nabla T) &= 0 \ , \ \mathrm{in}\Omega \\
\lambda\cdot\frac{\partial T}{\partial n} &= T-T^* \ , \ \mathrm{on}\partial\Omega,
\end{aligned}$$

then (3.15) gives $\delta E = \delta E_1 + \delta E_2$ with

$$\delta E_1 = \epsilon\cdot\int_{\Omega}\lambda A(\phi,S_i)\cdot\tilde{\phi}\,\mathrm{d}\mathbf{x} + O(\epsilon^2), \tag{3.16}$$

$$\delta E_2 = \epsilon\cdot\int_{\Omega}\lambda B(\phi,S_i)\cdot\tilde{S}\,\mathrm{d}\mathbf{x} + O(\epsilon^2) \tag{3.17}$$

corresponding to the change of the mismatching energy due to $\tilde{\phi}$ and that due to $\tilde{S}$, respectively. Choosing

$$\begin{aligned}
\tilde{\phi}(\mathbf{x}) &= -\lambda(\mathbf{x})\cdot A(\phi(\mathbf{x}), S_i(\mathbf{x}))\,, \\
\tilde{S}(\mathbf{x}) &= -\lambda(\mathbf{x})\cdot B(\phi(\mathbf{x}), S_i(\mathbf{x}))\,,
\end{aligned}$$

and neglecting the $O(\epsilon^2)$ term, we have

$$\delta E \doteq -\epsilon\int_{\Omega}\lambda^2 A^2(\phi,S_i)\,\mathrm{d}\mathbf{x} - \epsilon\int_{\Omega}\lambda^2 B^2(\phi,S_i)\,\mathrm{d}\mathbf{x} \leq 0.$$

To conclude, we can reduce the mismatch energies by perturbing $\phi(\mathbf{x})$ and $S_i(\mathbf{x})$ using

$$\begin{aligned}
\phi^{\mathrm{new}}(\mathbf{x}) &= \phi^{\mathrm{old}}(\mathbf{x}) + \epsilon\tilde{\phi}(\mathbf{x}) \\
&= \phi^{\mathrm{old}}(\mathbf{x}) - \epsilon\lambda(\mathbf{x})\cdot A(\phi(\mathbf{x}), S_i(\mathbf{x}))\,, \qquad (3.18) \\
S_i^{\mathrm{new}}(\mathbf{x}) &= S_i^{\mathrm{old}}(\mathbf{x}) + \epsilon\tilde{S}(\mathbf{x}) \\
&= S_i^{\mathrm{old}}(\mathbf{x}) - \epsilon\lambda(\mathbf{x})\cdot B(\phi(\mathbf{x}), S_i(\mathbf{x}))\,, \qquad (3.19)
\end{aligned}$$

respectively.

3.3 Dealing with multiple point sources

In the above calculations, we have assumed that the data set $T^*|_{\partial\Omega}$ is collected on the boundary corresponding to the first-arrival of rays emanating from one single point source. In practice, we can perform such experiment multiple times to obtain multiple set of data with each set corresponds to rays emanating from one of those multiple point sources. Mathematically, we denote $T_j^*|_{\partial\Omega}$ the data set corresponding to the point source located at $\mathbf{x}_s^j$, $j = 1,2,3,\cdots N$. We can simply sum up all individual mismatch energy and minimize

$$E^N = \frac{1}{2}\sum_{j=1}^{N}\int_{\partial\Omega}\left|T_j - T_j^*\right|^2\mathrm{d}s,$$

where T_j is obtained by solving the eikonal equation (2.1) with the point source initial condition at $\mathbf{x}_s^j$. With almost the same calculation as above, the adjoint state equation for the j-th data set is given by

$$-\mathrm{div}(\lambda_j \nabla T_j) = 0 \text{ , in } \Omega \tag{3.20}$$

$$\lambda_j \cdot \frac{\partial T_j}{\partial n} = T_j - T_j^* \text{ , on } \partial\Omega. \tag{3.21}$$

The perturbations for the level set function $\phi(\mathbf{x})$ and the inner-region slowness $S_i(\mathbf{x})$ are given by

$$\tilde{\phi}(\mathbf{x}) = -\left(\sum_{j=1}^{N} \lambda_j\right) \cdot A(\phi, S_i) \text{ and}$$

$$\tilde{S}(\mathbf{x}) = -\left(\sum_{j=1}^{N} \lambda_j\right) \cdot B(\phi, S_i), \tag{3.22}$$

where $A(\phi, S_i)$ and $B(\phi, S_i)$ are given by (3.12) and (3.13), respectively. Once we have obtained these perturbations, we update the level set function and the slowness in the inner region by

$$\phi^{\mathrm{new}}(\mathbf{x}) = \phi^{\mathrm{old}}(\mathbf{x}) + \epsilon\tilde{\phi}(\mathbf{x}),$$
$$S_i^{\mathrm{new}}(\mathbf{x}) = S_i^{\mathrm{old}}(\mathbf{x}) + \epsilon\tilde{S}(\mathbf{x}).$$

3.4 Regularization of $\phi(\mathbf{x})$ and $S_i(\mathbf{x})$

In previous sections, we introduce the level set adjoint state method in which we invert for both the level set function $\phi(\mathbf{x})$ and the inner-region slowness $S_i(\mathbf{x})$. In our level set expression (3.4), $\phi(\mathbf{x})$ is set to be a signed distance function and $S_i(\mathbf{x})$ is assumed to be continuous. However, these properties cannot be automatically satisfied in the above reconstruction. Furthermore, since the inverse problem is highly ill-posed, it is necessary to impose extra regularization in both the level set perturbation and the update of the slowness.

For the level set function $\phi(\mathbf{x})$, we adopt the level set re-initialization. The idea is to keep ϕ a signed distance function without moving the zero level set. Mathematically, it can be achieved by solving the following system in an artificial time direction ξ up to the steady state

$$\frac{\partial \Phi}{\partial \xi} + \mathrm{sign}(\phi) \cdot (|\nabla \Phi| - 1) = 0, \tag{3.23}$$

$$\left.\frac{\partial \Phi}{\partial n}\right|_{\partial\Omega} = 0, \tag{3.24}$$

with the initial condition $\Phi|_{\xi=0} = \phi$ and $\mathrm{sign}(\phi) = \frac{2}{\pi}\arctan\phi$ is the signum function [34]. In practice, however, since we are interested in the solution only near the zero level set, there is no need to obtain the steady state solution. Instead, we simply solve the system for several $\Delta\xi$ steps (in our implementation usually 5 steps) and the intermediate solution Φ is used to replace the original level set function.

Other regularization procedure might also be used rather than the one we are proposing here. For example, one might also try to regularize the length of the boundaries by incorporating the total variation of ϕ, i.e. $\int |\nabla\phi|$, in the energy functional. In our current work however, we do not explore this possibility.

For the inner-region slowness $S_i(\mathbf{x})$, we smooth its corresponding perturbation $\tilde{S}(\mathbf{x})$ by solving

$$(I - \nu\Delta)\tilde{S}^* = \tilde{S} = -\left(\sum_{j=1}^{N} \lambda_j\right) \cdot B(\phi, S_i) \text{ , } in \ \Omega;$$

$$\frac{\partial \tilde{S}^*}{\partial n} = 0 \text{ , } on \ \partial\Omega \tag{3.25}$$

where I is the identity operator, Δ is the Laplace operator and $\nu > 0$ is the weighting controlling the amount of regularity one wants. Then $\tilde{S}^*$ is used to replace $\tilde{S}$ as the perturbation to $S_i(\mathbf{x})$. With this

particular perturbation, the decrease in the mismatching energy due to $\tilde{S}^*$ follows

$$\begin{aligned}\delta E_2 &\doteq \epsilon \cdot \int_\Omega \left(\sum_{j=1}^N \lambda_j\right) \cdot B(\phi, S_i) \cdot \tilde{S}^* \,\mathrm{d}\mathbf{x} \\ &= -\epsilon \cdot \int_\Omega (I - \nu\Delta)\tilde{S}^* \cdot \tilde{S}^* \,\mathrm{d}\mathbf{x} \\ &= -\epsilon \cdot \int_\Omega \left((\tilde{S}^*)^2 + \nu \left|\nabla \tilde{S}^*\right|^2\right) \mathrm{d}\mathbf{x} \leq 0.\end{aligned}$$

4 Simplification for piecewise homogeneous structure

In the previous derivations we are interested in the media with **piecewise-continuous** slowness. In this section we consider a simpler case where the media has piecewise-homogeneous, yet **unknown**, slowness. That is, the outer-region slowness $S_o(\mathbf{x}) = S_o$ and the inner-region slowness $S_i(\mathbf{x}) = S_i$ are just constants. In particular, we follow the same approach as in the previous section. We express the slowness using the level set expression (3.4) while treating the constant S_o as a given constant and S_i is an unknown.

Recall formula (3.17) which relates the change in the mismatching energy $E(\phi, S_i)$ and the perturbation $\tilde{S}(\mathbf{x})$ on the inner-region slowness. For piecewise-homogeneous structure, S_i is restricted to be constant, a natural consideration is to improve a constant initial guess of S_i by a constant perturbation parameter $\tilde{S}$. Then the descent direction for $\tilde{S}$ is given by

$$\tilde{S} = -\int_\Omega \lambda B(\phi, S_i) \,\mathrm{d}\mathbf{x},$$

which leads to

$$\delta E_2 \doteq -\epsilon \cdot \left[\int_\Omega \lambda B(\phi, S_i) \,\mathrm{d}\mathbf{x}\right]^2 \leq 0.$$

For the multiple data sets as mentioned in Section 3.3, the descent direction for $\tilde{S}$ is

$$\tilde{S} = -\int_\Omega \left(\sum_{j=1}^N \lambda_j\right) \cdot B(\phi, S_i) \,\mathrm{d}\mathbf{x}, \tag{4.26}$$

where $B(\phi, S_i)$ is given by (3.13). Finally S_i is updated by $S_i^{\text{new}} = S_i^{\text{old}} + \epsilon\tilde{S}$. Note in this case no regularization in the perturbation is necessary and so we do not smooth the perturbation $\tilde{S}$ anymore.

It is worth noticing an interesting recent work in [59] which further simplifies this tomography problem by assuming that both inside and outside slowness are **known**, which essentially reduces the inverse problem to a shape optimization problem. In particular, one can obtain the formulation in [59] by restricting both constants S_o and S_i in our derivation to be given constants. For instance, in expression (3.4), $S(\mathbf{x})$ is solely determined by the level set function $\phi(\mathbf{x})$. To invert for the slowness distribution $S(\mathbf{x})$, one only need to obtain the level set function $\phi(\mathbf{x})$ using the methodology described in Section 3.2. In [59], however, no derivation of the functional derivative is given. And it has no discussion on how the regularity in smoothing the Heaviside function affects the convergence in minimizing the functional.

5 Numerical implementation

5.1 Full level set implementation

In this section, we summarize the above algorithm on inverting a piecewise continuous slowness and also discuss the numerical implementation in details.

Algorithm: Level set adjoint state method for transmission traveltime tomograph with discontinuous slowness.

1. Initialize ϕ^k and S_i^k for $k = 0$.
2. Construct $S(\mathbf{x})$ using (3.4).

3. Solve the eikonal equation (2.1) with the point source condition (2.2), and obtain $T_j(\mathbf{x})$ for each data set, $j=1,2,3,\cdots N$.
4. Obtain $\lambda_j(\mathbf{x})$ by solving the adjoint state equations (3.20), (3.21) for $j=1,2,3,\cdots N$.
5. Compute $\tilde{\phi}^k(\mathbf{x})$ and $\tilde{S}^k(\mathbf{x})$ using the formula (3.22).
6. Update $\phi^{k+1}=\phi^k+\epsilon\cdot\tilde{\phi}^k$. Then re-initialize the level set function following the procedure provided in Section 3.4, use Φ to update ϕ^{k+1}.
7. Smooth the perturbation parameter $\tilde{S}^k(\mathbf{x})$ following the procedure provided in Section 3.4, and update $S_i^{k+1}(\mathbf{x})=S_i^k(\mathbf{x})+\epsilon\cdot\tilde{S}^*(\mathbf{x})$.
8. Go back to step 2 until the mismatching energy $E\leq\delta$ or the iteration step $k\geq k_{\max}$ for some given convergence parameters δ and $k_{\max}$.

In step (iii), we solve the eikonal equation using the fast sweeping method [58]. Since such finite difference scheme is monotonic in $S(\mathbf{x})$ and it converges to the viscosity solution of eikonal equation for a continuous $S(\mathbf{x})$, this simple numerical scheme also converges to the extended viscosity solution for piecewise continuous slowness $S(\mathbf{x})$ [24]. If necessary, one might also use some recently developed fast sweeping method for more accurate results [19, 31]. In this paper, on the other hand, we do not pursue this direction for a more accurate forward solution. For step (iv), we compute λ by solving the adjoint state equation. A detailed numerical discretization description can be found in [28].

In step (vi), the reinitialization equation is a first order nonlinear hyperbolic Hamilton-Jacobi equation. One can apply the TVDRK3 [46] in the time direction and the WENO5 [23] for the spatial derivative. This could give a high order accurate solution to the ξ-direction evolution. The CFL condition for solving this equation is given by $\Delta t<CFL\cdot\Delta x$. If only low order solution is needed, one may simply replace the TVDRK3 by a forward Euler step and the WENO5 by the simple forward/backward differencing.

The above algorithm is designed for inverting a piecewise-continuous structure, where $S_i(\mathbf{x})$ is an unknown continuous function. For piecewise-homogeneous structure described in Section 4, S_i is assumed to be constant and we only need to slightly modify the algorithm. For instance, in step (i), the initialization for S_i^0 is chosen to be $S_i^0=C$, where C is a positive constant. In step (v), $\tilde{S}^k$ is computed using expression (4.26), and S_i is directly updated by $S_i^{k+1}=S_i^k+\epsilon\cdot\tilde{S}^k$ without the regularization in step (vii). Moreover, as mentioned in Section 4, if both S_o and S_i are assumed to be known, we do not need to initialize S_i^0 in step (i) and there is no need to compute $\tilde{S}^k$ in step (vii) at all.

5.2 Local level set implementation

To further improve the computational complexity, we propose to replace the above full level set implementation by incorporating the fast local level set method proposed in [37]. Since we only care about the location of the zero level set in the discontinuity representation, we propose to follow the local level set method by updating the level set function only in a neighborhood of the zero level set.

The fundamental idea in the local level set method consists of two components. One is to update the level set function only in a small neighborhood of the zero level set. This step helps to improve the computational time since we do not need to determine $\tilde{\phi}(\mathbf{x})$ and $\phi^{\text{new}}(\mathbf{x})$ in (3.18) for all locations in the whole computational domain, but instead grid points near a co-dimensional one surface. The next step in the local level set method requires to update the computational tube $\{\mathbf{x}:|\phi(\mathbf{x})|<\epsilon_{\text{local}}\}$ as the interface evolves in time. Since we have already regularized the evolution using the reinitialization equation (3.24), the signed distance value of the level set function can be used to determine the computational tube at the next time step. So this step requires no extra computational power.

6 Numerical examples

In this section, we consider various examples to demonstrate the effectiveness of the level set formulation for first arrival transmission traveltime tomography. In Section 6.1, we first consider the simplest case where both the inside and the outside slowness are **known** constants. This results in just a shape optimization problem. Then in Section 6.2, we assume that the inside slowness is an **unknown** constant

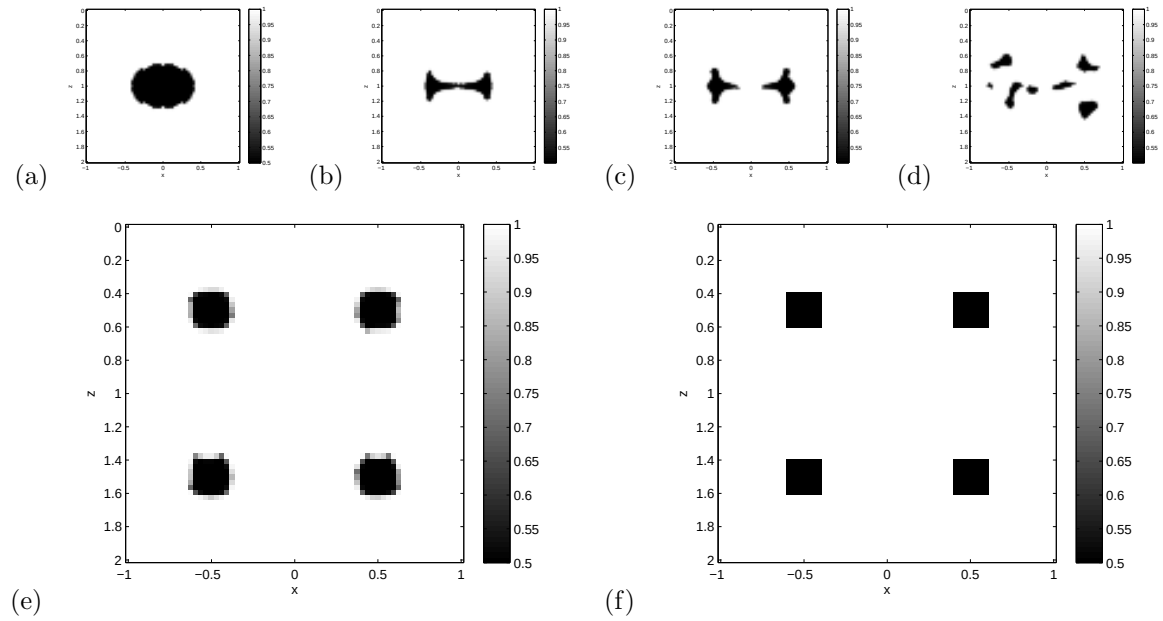

Figure 2: (Section 6.1) Both S_0 and S_i are assumed to be known constants. (a-d) Some intermediate solutions in the level set evolution. (e) Our final solution. (f) Exact solution.

and so S_i will be a part of the inverse problem. Finally, we will consider the difficult case by treating S_i to be a continuous function in Section 6.3. In these numerical experiments unless specified otherwise, the computational domain is set to be $\Omega=[-1,1]\times[0,2]$ and we use 65×65 mesh grids. The smoothing parameter τ is chosen to be $\tau=0.01$, and the width of the computational tube for the local level set implementation is $\epsilon_{\text{local}}=4\Delta x$. 14 point sources are used, half of which are uniformly distributed on $z=0.1$ and the other half are put on $z=1.9$. Unless otherwise specified, we assume receivers are all placed on the boundary of the computational domain. The initial guess for the level set function $\phi(x,z)$ is the signed distance function to $x^2+(z-1)^2=0.81$.

6.1 Both S_o and S_i are known

In this first example, we consider the slowness

$$S(\mathbf{x})=\begin{cases}0.5\ ,\ |x+0.5|\le0.1 \text{ and } |z-0.5|\le0.1\\ 0.5\ ,\ |x+0.5|\le0.1 \text{ and } |z-1.5|\le0.1\\ 0.5\ ,\ |x-0.5|\le0.1 \text{ and } |z-1.5|\le0.1\\ 0.5\ ,\ |x-0.5|\le0.1 \text{ and } |z-0.5|\le0.1\\ 1\ ,\ \text{otherwise.}\end{cases}$$

The perturbation parameter for $\phi(\mathbf{x})$ is chosen to be $\epsilon=6\times10^{-3}$ and we perform the iterative inversion process for 500 steps. The results are shown in Figure 2. We have also plotted several intermediate solutions in our inversion process. The level set representation can naturally handle the topological change from the initial circle to the final four disjoint square shapes. This is a relatively simple case since the function S_i is assumed to be a given constant and so the inverse problem is just a shape optimization problem written in the level set framework.

6.2 Piecewise-homogeneous structure

In this subsection we assume that $S_i(\mathbf{x})$ is unknown yet restricted to be a constant S_i. We choose two different initial guesses for S_i, $S_i^0=0.1$ and $S_i^0=0.9$. We have tested the algorithm on two piecewise constant configurations. The first one consists of two disjoint objects given by

$$S(\mathbf{x})=\begin{cases}0.5\ ,\ |x-0.5|\le0.3 \text{ and } |z-1.5|\le0.3\\ 0.5\ ,\ (x+0.5)^2+(z-0.5)^2\le0.25^2\\ 1\ ,\ \text{otherwise}\end{cases},$$

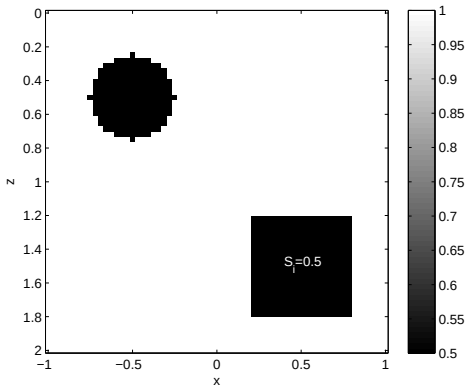

(a) Exact slowness

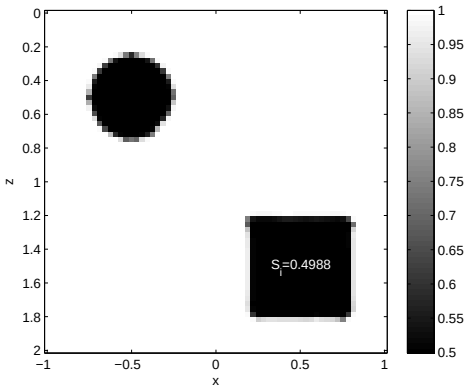

(b) Piecewise-homogeneous reconstruction, $S_i^0 = 0.1$

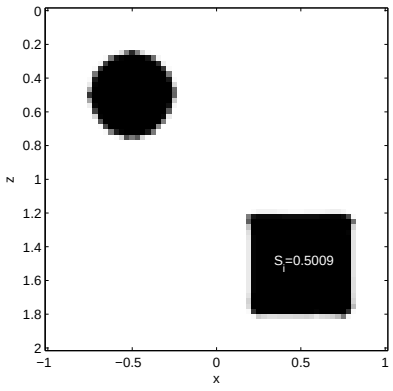

(c) Piecewise-homogeneous reconstruction, $S_i^0 = 0.9$

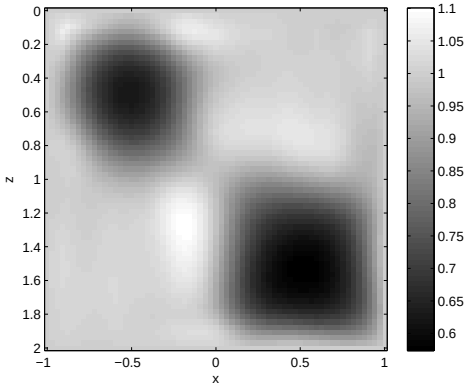

(d) Smooth reconstruction

Figure 3: (Section 6.2) S_i is assumed to be an unknown constant. (a)-(c) Results using piecewise-homogeneous reconstruction. The inverted constant S_i is marked on the figure. (d) Results using smooth reconstruction.

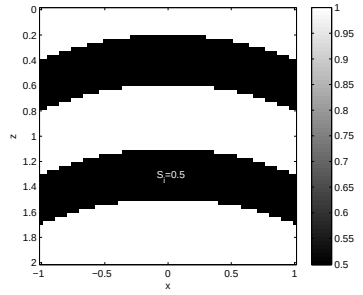

(a) Exact slowness

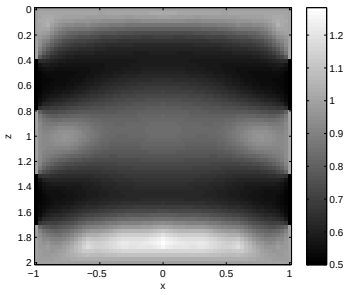

(b) Smooth reconstruction

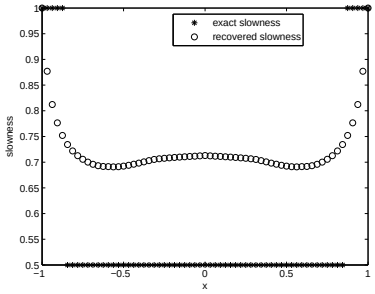

(c) Cross-section of (b) along $z = 1.25$

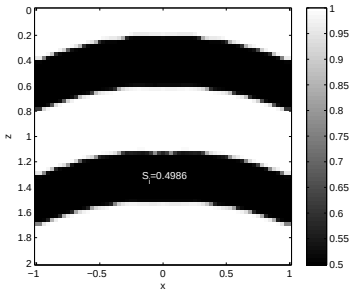

(d) Reconstruction with $S_i^0 = 0.1$

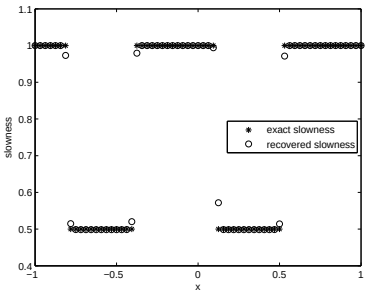

(e) Cross-section of (d) along $x = 0$

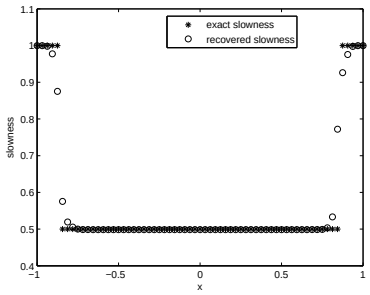

(f) Cross-section of (d) along $z = 1.25$

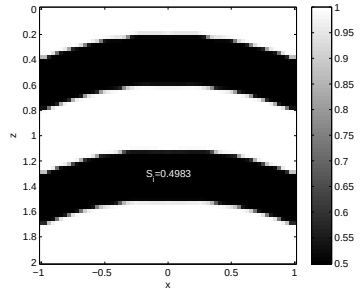

(g) Reconstruction with $S_i^0 = 0.9$

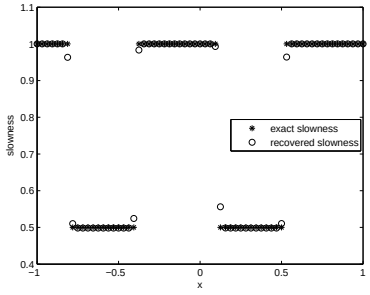

(h) Cross-section of (g) along $x = 0$

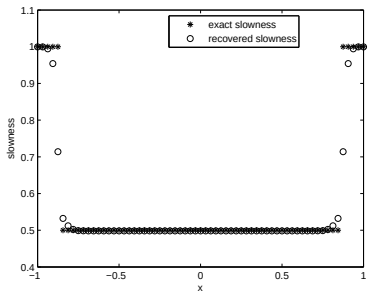

(i) Cross-section of (g) along $z = 1.25$

Figure 4: (Section 6.2) S_i is assumed to be an unknown constant. (b,d,e) Results using piecewise-homogeneous reconstruction. The inverted constant S_i is marked on the figure. (c,f) Results using smooth reconstruction.

and the second one is a layer structure given by

$$S(\mathbf{x}) = \begin{cases} 0.5 \ , \ \Omega_i \\ 1 \ , \ \text{otherwise,} \end{cases}$$

where $\Omega_i = \{(x,z) : 3.7 - \sqrt{2.6^2 - x^2} \le z \le 4.1 - \sqrt{2.6^2 - x^2}$ and $2.8 - \sqrt{2.6^2 - x^2} \le z \le 3.2 - \sqrt{2.6^2 - x^2}\}$. In both of these examples, the perturbation parameter is chosen to be 6×10^{-3}. For the first profile, we perform 1500 iterations for both initial conditions. For the layer structure, we perform 5000 and 15000 iterations for the cases $S_i^0 = 0.1$ and 0.9, respectively. Figure 3 and Figure 4 show the numerical results. In our piecewise-homogeneous reconstruction the sharp structures are well recovered. The estimated S_i in these examples are approximately 0.4988, 0.5009, 0.4986 and 0.4983, respectively, which match extremely well with the exact value 0.5. As a comparison we also present the smooth reconstructions using the method in our previous work [28]. The solution here is much improved by the level set formulation.

6.3 Piecewise-continuous structure

In this subsection we consider the general case where $S_i(\mathbf{x})$ is an unknown continuous function. The inverse problem is to invert both $S_i(\mathbf{x})$ and the level set function $\phi(\mathbf{x})$ for the discontinuity location Γ. In the inversion procedure, we regularize the flow by choosing ν in equation (3.25) to be unity. The initial guess for the level set function $\phi(x,z)$ is still the signed distance to $x^2 + (z-1)^2 = 0.81$, and the initial guess for $S_i(x,z)$ is S_i^0 satisfying

$$\begin{aligned} (I - \nu\Delta) S_i^0 &= 0 \ , \ \mathbf{x} \in \Omega \\ S_i^0 &= 0.8 \ , \ \mathbf{x} \in \partial\Omega. \end{aligned}$$

In the first case, the exact slowness is given by

$$S(\mathbf{x}) = \begin{cases} S_i(\mathbf{x}) \ , \ |x| \le 0.5 \text{ and } |z-1| \le 0.5 \\ 1 \ , \ \text{otherwise} \end{cases}.$$

We have tested on slowness given by $S_i(x,z) = |x|^3 + |z-1|^3 + 0.5$. In this example we set the perturbation parameter $\epsilon = 5 \times 10^{-3}$, and the maximum number of iterations is 30000. Figure 5 (b) shows the numerical results. For comparison still we present the smooth reconstructions using the method in our previous work [28], the results are shown in Figure 5 (c) and (f).

To further test the robustness of the algorithm, we have repeated the experiment but have perturbed the measurements T^* by a 1% Gaussian noise with zero mean. The results are shown in Figure 6. In our reconstruction the error mainly occurs at the location of the discontinuity while the profile of the inside region and the related slowness $S_i(\mathbf{x})$ are well recovered.

In the second case, we consider the layer structure where the exact slowness is given by

$$S(\mathbf{x}) = \begin{cases} S_i(\mathbf{x}) \ , \ \Omega_i \\ 1 \ , \ \text{otherwise} \end{cases}.$$

and $S_i(x,z) = 0.25x^3 + 0.5$ and $\Omega_i = \{(x,z) : 3.7 - \sqrt{2.6^2 - x^2} \le z \le 4.1 - \sqrt{2.6^2 - x^2}$ or $2.8 - \sqrt{2.6^2 - x^2} \le z \le 3.2 - \sqrt{2.6^2 - x^2}\}$. The perturbation parameter is still set to be $\epsilon = 5 \times 10^{-3}$ and we take a maximum of 30000 iterations.

Figure 7 shows the numerical results using the piecewise-continuous reconstruction. Like previous examples, the error would be in the location of the discontinuity with almost exact inverted slowness in the inside region Ω_i. As a comparison, we also present the inverted solutions using the piecewise-homogeneous reconstruction and the smooth reconstruction, the results are shown in Figure 8. It illustrates that for this complicated structure, piecewise-continuous reconstruction is necessary and gives better solutions.

6.4 Structures generated from the Marmousi model

In this last example, we consider some complicated profiles generated from the Marmousi model. The original Marmousi model is sampled on a 0.024km by 0.024km mesh, consisting of 384 samples in the x-direction and 122 samples in the z-direction; where $x \in [0, 9.192\text{km}]$ and $z \in [0, 2.904\text{km}]$. Let $S_{\text{Marmousi}}(x,z)$ be the slowness distribution of the Marmousi model. In the following we also introduce the notation $C(x,z)$ for the velocity, such that $C_{\text{Marmousi}}(x,z) = [S_{\text{Marmousi}}(x,z)]^{-1}$.

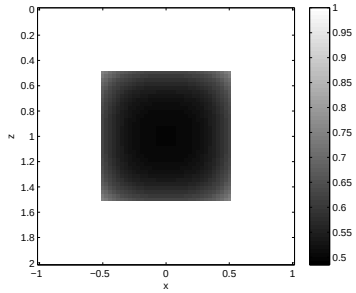

(a) $S_i(x,z) = |x|^3 + |z-1|^3 + 0.5$

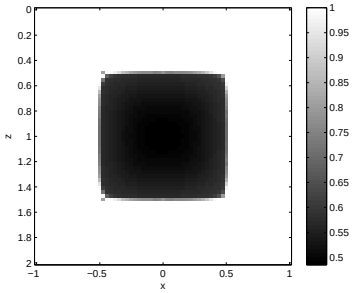

(b) Piecewise-continuous reconstruction

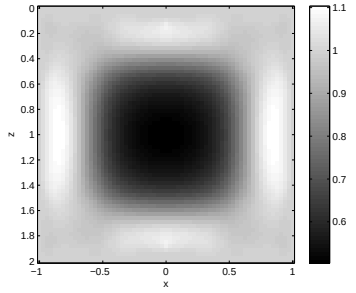

(c) Smooth reconstruction

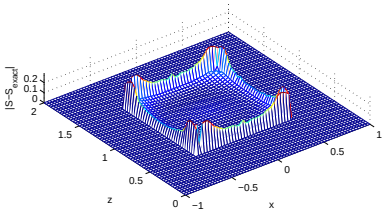

(d) Error in $S(x,z)$ from (b)

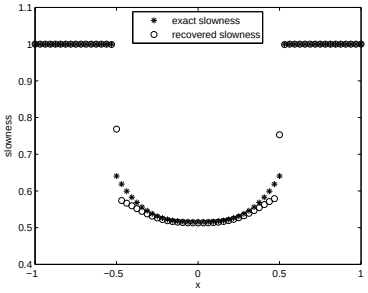

(e) Cross-section of (b) along $z = 0.75$

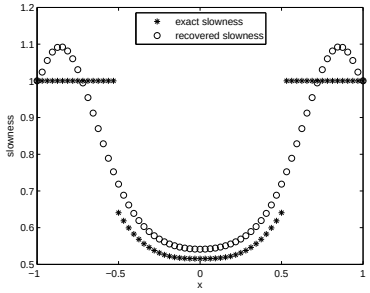

(f) Cross-section of (c) along $z = 0.75$

Figure 5: (Section 6.3) S_i is assumed to be an unknown continuous function with the exact solution given by $S_i(x,z) = |x|^3 + |z-1|^3 + 0.5$. (b,d,e) Results using piecewise-continuous reconstruction. (c,f) Results using smooth reconstruction.

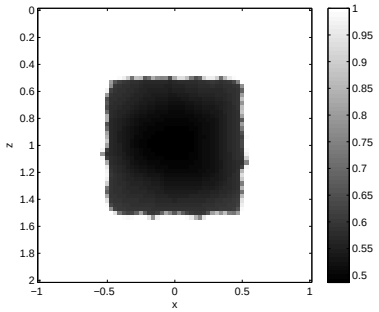

(a) Recovered slowness using measurements with noise, $S_i = |x|^3 + |z-1|^3 + 0.5$

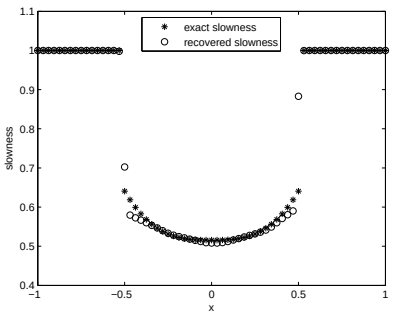

(b) Cross-section along $z = 0.75$

Figure 6: (Section 6.3) Numerical results using measurements with noise, S_i is assumed to be an unknown continuous function with $S_i(x,z) = |x|^3 + |z-1|^3 + 0.5$.

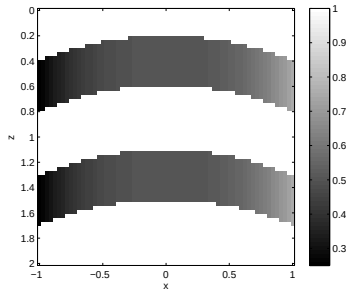

(a) $S_i(x,z) = 0.25x^3 + 0.5$

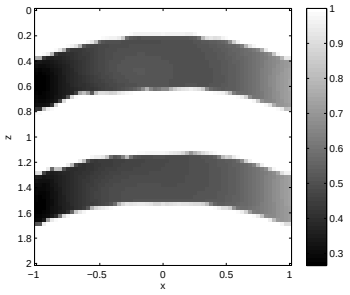

(b) Piecewise-continuous reconstruction

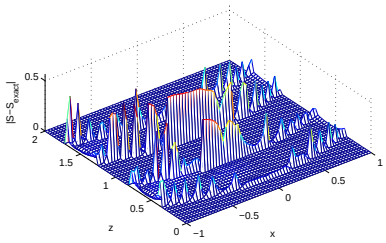

(c) Error in $S(x,z)$ from (b)

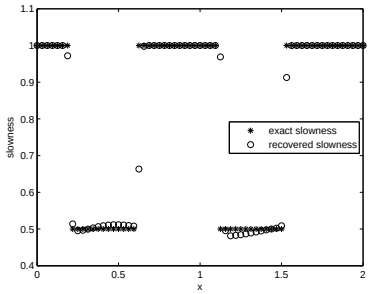

(d) Cross-section of (b) along $x = 0$

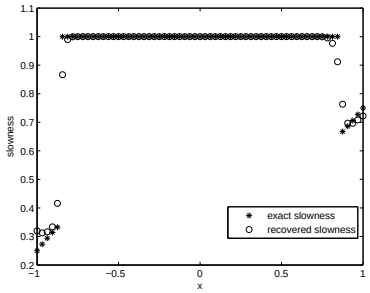

(e) Cross-section of (b) along $z = 0.75$

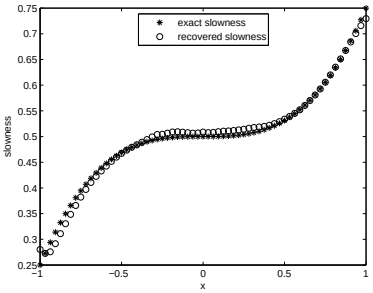

(f) Cross-section of (b) along $z = 1.5$

Figure 7: (Section 6.3) Results using piecewise-continuous reconstruction, the inside slowness S_i is assumed to be an unknown continuous function.

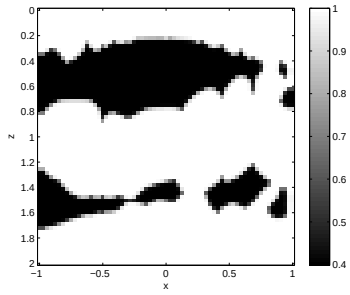

(a) Piecewise-homogeneous reconstruction

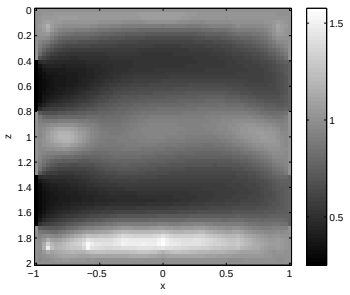

(b) Smooth reconstruction

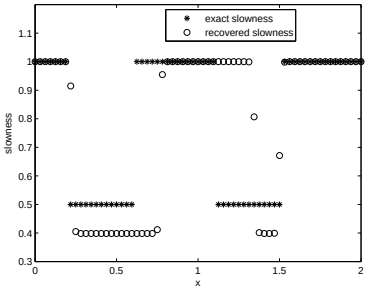

(c) Cross-section of (a) along $x=0$

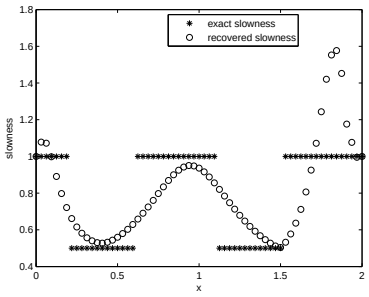

(d) Cross-section of (b) along $x=0$

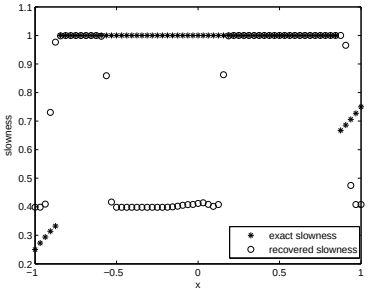

(e) Cross-section of (a) along $z=0.75$

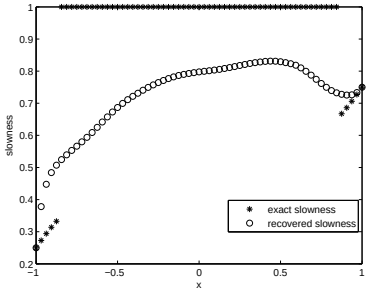

(f) Cross-section of (b) along $z=0.75$

Figure 8: (Section 6.3) $S_i(x,z)=0.25x^3+0.5$. (a),(c),(e) Results using piecewise-homogeneous reconstruction. (b),(d),(f) Results using smooth reconstruction.

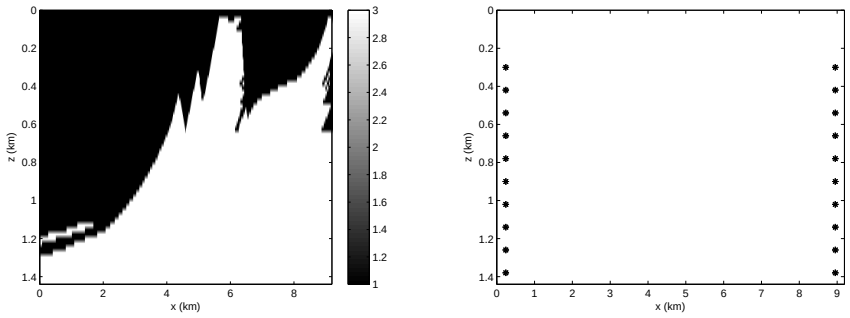

(a) $C_1(x,z)$ (b) Source locations

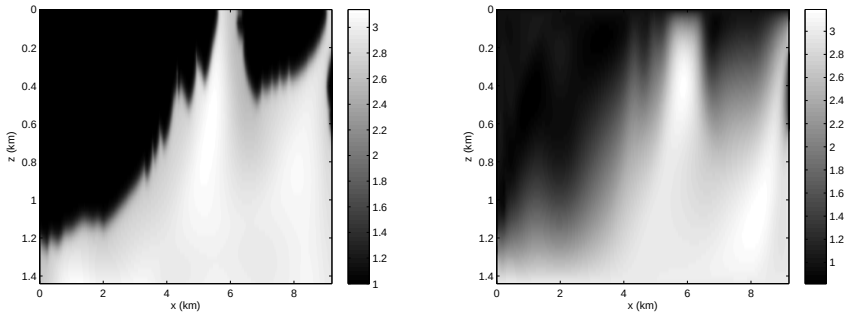

(c) Piecewise-continuous reconstruction (d) Smooth reconstruction

Figure 9: (Section 6.4)Results for $C_1(x,z)$. The demonstrated parameter is the velocity rather than the slowness.

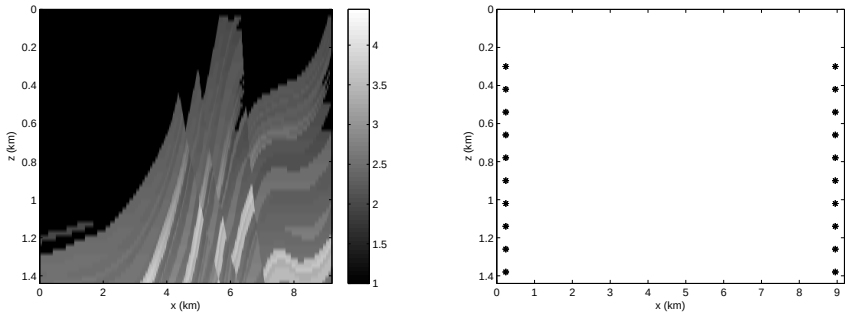

(a) $C_2(x,z)$ (b) Source locations

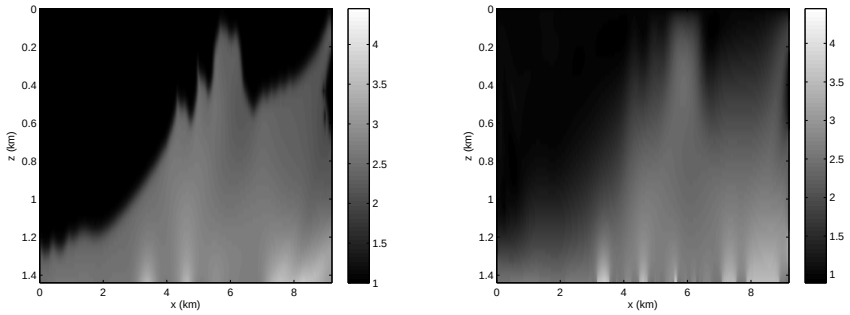

(c) Piecewise-continuous reconstruction (d) Smooth reconstruction

Figure 10: (Section 6.4)Results for $C_2(x,z)$.

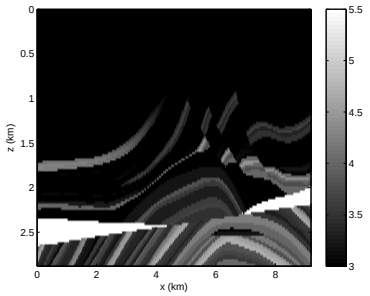

(a) $C_3(x,z)$

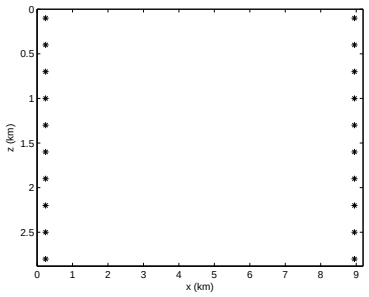

(b) Source locations

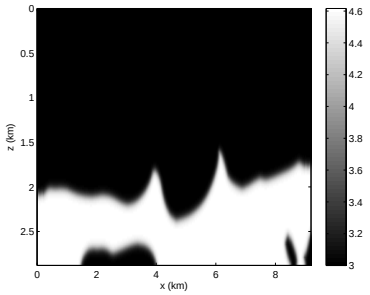

(c) Piecewise-homogeneous reconstruction

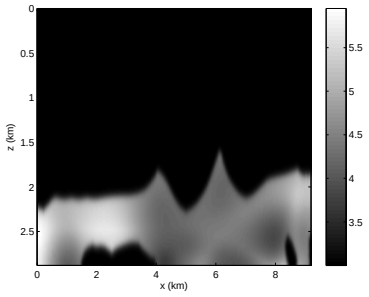

(d) Piecewise-continuous reconstruction

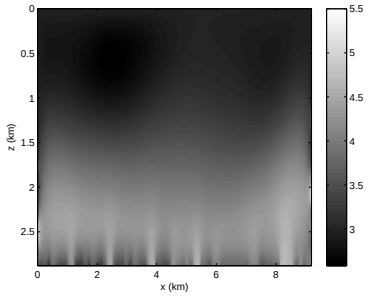

(e) Smooth reconstruction

Figure 11: (Section 6.4)Results for $C_3(x,z)$. The result in (c) is used as an initial guess to get the result in (d).

We have studied three different profiles. The first two structures are in the region $x\in[0,9.192\text{km}]$ and $z\in[0,1.44\text{km}]$, which is half part of the region of the original Marmousi model; they are given by

$$C_1(x,z)=\begin{cases}1\ , \text{ if } C_{\text{Marmousi}}(x,z)\le 2\\ 3\ , \text{ otherwise}\end{cases},$$

and

$$C_2(x,z)=\begin{cases}1 & , \text{ if } C_{\text{Marmousi}}(x,z)\le 2\\ C_{\text{Marmousi}}(x,z) & , \text{ otherwise}\end{cases}.$$

Figure 9 and Figure 10 show the profiles with our inverted solutions. In these two examples, we use 20 sources which are distributed on $(x=0.24,z=0.3:0.12:1.38)$ and $(x=8.952,z=0.3:0.12:1.38)$. The outside slowness S_o is assumed to be known value given by $S_o(x,z)=1$ and the initial guess for the inside slowness is $S_i(x,z)=S_o(x,z)/2$. Also the initial guess for the level set function ϕ is chosen as the singed distance function to $(x-4.596)^2/4^2+(z-0.77)^2/0.6^2=1$. We set the smoothing parameter τ to be $\tau=0.05$, and the perturbation parameter for ϕ and S_i is $\epsilon=10^{-3}$. 3000 iterations lead to Figure 9(c) and 20000 iterations lead to Figure 10(c). For comparison we also present the results using smooth reconstruction in our previous work [28], they are shown in Figures 9(d) and 10(d) respectively.

The third structure is given in the region $(x,z)\in[0,9.192\text{km}]\times[0,2.88\text{km}]$ by

$$C_3(x,z)=\begin{cases}3 & , \text{ if } C_{\text{Marmousi}}(x,z)\le 3\\ C_{\text{Marmousi}}(x,z) & , \text{ otherwise}\end{cases}.$$

The numerical results are shown in Figure 11. In the computation we use 20 sources sampled on $(x=0.24,z=0.1:0.3:2.8)$ and $(x=8.952,z=0.1:0.3:2.8)$. The outside slowness S_o is a known value given by $S_o(x,z)=1/3$ and the initial guess for the inside slowness is $S_i(x,z)=S_o(x,z)/2$. Also the initial guess for the level set function ϕ is the singed distance function to $(x-4.596)^2/4^2+(z-1.44)^2/1.3^2=1$. Still we set the smoothing parameter τ to be $\tau=0.05$, and the perturbation parameter for ϕ and S_i is $\epsilon=10^{-3}$. In the inverted solution, firstly we use a piecewise-homogeneous reconstruction that the inside slowness S_i is assumed to be constant, a preliminary result after 7500 iterations is given in Fig 11(c). And then this preliminary result is set to be an initial guess and the piecewise-continuous reconstruction is performed, the result after 3000 iterations is shown in Fig 11(d). For comparison Figure 11(e) also presents the result using the smooth reconstruction.

7 Limitation and discussion

In this paper, we propose a local level set formulation for first arrival transmission traveltime tomography with discontinuous slowness based on the adjoint state techniques. Even though the numerical examples in the previous section have demonstrated extremely good results, there is limitation of the proposed method. To illustrate the problem, we consider the following discontinuous slowness given by

$$S(\mathbf{x})=\begin{cases}1\ , |x|\le 0.5 \text{ and } |z-1|\le 0.5\\ 0.5\ , \text{otherwise}\end{cases}.$$

The location of the discontinuity is the same as the example in Figure 5. The difference is that the outside slowness has a smaller value than that of the inside region. In Figure 12 (a-b), we have shown the slowness together with the quantity $\nabla T/|\nabla T|$ where T is obtained by solving the eikonal equation with the point source located at the origin. Since the characteristics of the eikonal equation (2.1) is given by $\mathrm{d}\mathbf{x}/\mathrm{d}s=\frac{\nabla T}{S^2}$, the quantity $\nabla T/|\nabla T|$ gives the ray direction. We observe that rays reaching the receivers on the boundary carry no information from the inner region at all.

We have tried our algorithm on this structure with both S_i and S_o assumed to be known. The use of point sources and the initial condition for the level set function are the same as before, and the perturbation parameter is set to be $\epsilon=6\times10^{-3}$. We have plotted our inverted solution after 10000 iterations in Figure 12 (c) with the corresponding ray directions shown in Figure 12 (d). As demonstrated in our previous works [28, 29], a possible way to improve the solution of this kind is to consider the multiple-arrival transmission traveltime tomography which provides more information of the rays in the inverse problem.

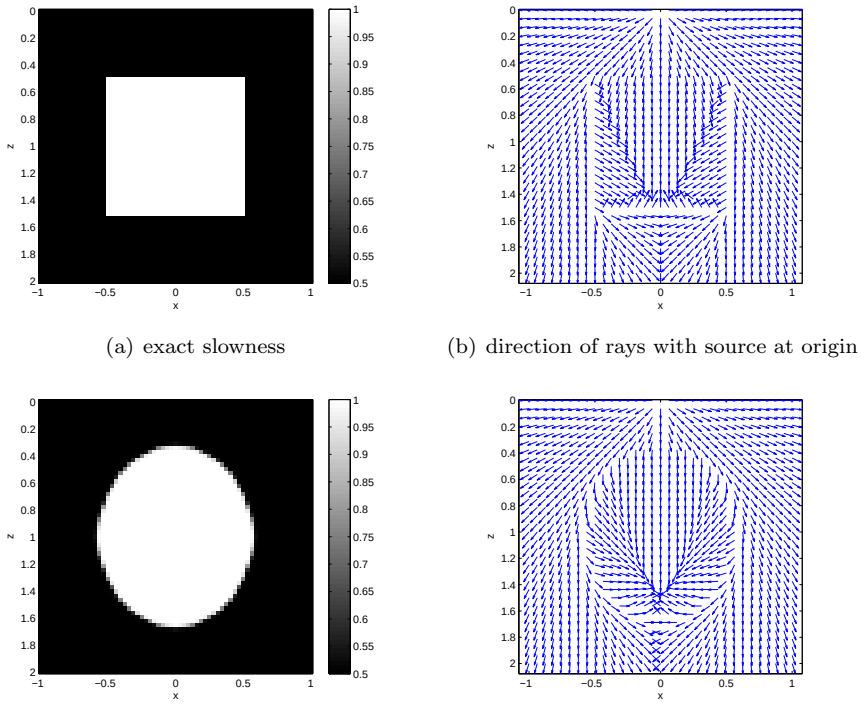

(a) exact slowness (b) direction of rays with source at origin

(c) recovered slowness (d) direction of rays with source at origin

Figure 12: Limitation of the proposed algorithm.

ACKNOWLEDGMENTS

Some preliminary results in the paper were presented by Li in the SIAM Annual Meeting 2012 but none of them has yet been published. Li is supported in part by the Hong Kong PhD Fellowship. Leung is supported in part by the Hong Kong RGC under Grant GRF603011.

References

[1] J. Berryman. Analysis of approximate inverses in tomography I. resolution analysis of common inverses. *Optimization and Engineering*, 1:87–115, 2000.

[2] J. Berryman. Analysis of approximate inverses in tomography II. iterative inverses. *Optimization and Engineering*, 1:437–473, 2000.

[3] T. N. Bishop, K. P. Bube, R. T. Cutler, R. T. Langan, P. L. Love, J. R. Resnick, R. T. Shuey, D. A. Spindler, and H. W. Wyld. Tomographic determination of velocity and depth in laterally varying media. *Geophysics*, 50:903–923, 1985.

[4] P. Bois, M.L. Porte, M. Levergne, and G. Thomas. Well-to-well seismic measurements. *Geophysics*, 37:471–480, 1972.

[5] M. Burger. A level set method for inverse problems. *Inverse Problems*, 17:1327–1356, 2001.

[6] M. Burger and S. Osher. A survey on level set methods for inverse problems and optimal design. *European J. Appl. Math.*, 16:263–301, 2005.

[7] V. Cerveny. *Seismic ray tracing*. Cambridge University Press, 2001.

[8] G. Chavent. Identification of function parameters in partial differential equations. *Identification of parameter distributed systems*, eds Goodson, R.E. & Polis, New York, ASME, 1974.

[9] E. Chung, T.F. Chan, and X.-C. Tai. Electrical impedance tomography using level set representation and total variational regularization. *J. Comput. Phys.*, 205:357–372, 2005.

[10] E. Chung, J. Qian, G. Uhlmann, and H. Zhao. A new phase space method for recovering index of refraction from travel times. *Inverse Problems*, 23:309–329, 2007.

[11] E. Chung, J. Qian, G. Uhlmann, and H. Zhao. A phase-space formulation for elastic-wave traveltime tomography. *J. Phys.: Conf. Ser.*, 124:012018, 2008.

[12] E. Chung, J. Qian, G. Uhlmann, and H. Zhao. An adaptive phase space method with application to reflection traveltime tomography. *Inverse Problems*, 27:115002, 2011.

[13] R. A. Clarke, B. Alazard, L. Pelle, D. Sinuquet, P. Lailly, F. Delprat-Jannaud, and L. Jannaud. 3D traveltime reflection tomography with multi-valued arrivals. In *71st Ann. Internat. Mtg., Soc. Expl. Geophys., Expanded Abstracts*, pages 1601–1604. Soc. Expl. Geophys., Tulsa, OK, 2001.

[14] M. G. Crandall and P. L. Lions. Viscosity solutions of Hamilton-Jacobi equations. *Trans. Amer. Math. Soc.*, 277:1–42, 1983.

[15] K. Deckelnick and C.M. Elliott. Uniqueness and error analysis for Hamilton-Jacobi equations with discontinuities. *Interface and Free Boundaries*, 6:329–349, 2004.

[16] K. Deckelnick, C.M. Elliott, and V. Styles. Numerical analysis of an inverse problem for the eikonal equation. *Numer. Math.*, 119:245–269, 2011.

[17] F. Delprat-Jannaud and P. Lailly. Reflection tomography: how to handle multiple arrivals? *J. Geophys. Res.*, 100:703–715, 1995.

[18] O. Dorn and D. Lesselier. Level set methods for inverse scattering. *Inverse Problems*, 22:67–131, 2006.

[19] S. Fomel, S. Luo, and H. Zhao. Fast sweeping method for the factored eikonal equation. *J. Comput. Phys.*, 228:6440–6455, 2009.

[20] J.-W. Huang and G. Bellefleur. Joint transmission and reflection traveltime tomography using the fast sweeping method and the adjoint-state technique. *Geophysical J. Inter.*, 188:570–582, 2012.

[21] V. Isakov, S. Leung, and J. Qian. A fast local level set method for inverse gravimetry. *Commun. Comput. Phys.*, 10:1044–1070, 2011.

[22] V. Isakov, S. Leung, and J. Qian. Inverse gravimetry problem for ice with snow caps. *In Preparation*, 2012.

[23] G. S. Jiang and D. Peng. Weighted ENO schemes for Hamilton-Jacobi equations. *SIAM J. Sci. Comput.*, 21:2126–2143, 2000.

[24] J. Kain and D.N. Ostrov. Numerical shape-from-shading for discontinuous photographic images. *Int. J. of Comp. Vis.*, 44:163–173, 2001.

[25] C. Y. Kao, S. J. Osher, and Y.-H. Tsai. Fast sweeping method for static Hamilton-Jacobi equations. *SIAM J. Num. Anal.*, 42:2612–2632, 2005.

[26] P.G. Lelievre, C.G. Farquharson, and C.A. Hurich. Inversion of first-arrival seismic traveltimes without rays, implemented on unstructured grids. *Geophysical J. Inter.*, 185:749–763, 2011.

[27] S. Leung and J. Qian. A transmission tomography problem based on multiple arrivals from paraxial liouville equations. *Expanded Abstract for the SEG 75th Annual Meeting*, 2005.

[28] S. Leung and J. Qian. An adjoint state method for 3d transmission traveltime tomography using first arrival. *Commun. Math. Sci.*, 4:249–266, 2006.

[29] S. Leung and J. Qian. Transmission traveltime tomography based on paraxial liouville equations and level set formulations. *Inverse Problems*, 23:799–821, 2007.

[30] A. Litman, D. Lesselier, and F. Santosa. Reconstruction of a 2-d binary obstacle by controlled evolution of a level-set. *Inverse Problems*, 14:685–706, 1998.

[31] S. Luo and J. Qian. Factored singularities and high-order Lax-Friedrichs sweeping schemes for point-source traveltimes and amplitudes. *J. Comput. Phys.*, 230:4742–4755, 2011.

[32] S. M. Minkoff. A computationally feasible approximate resolution matrix for seismic inverse problems. *Geophys. J. Int.*, 126:345–359, 1996.

[33] R. Montelli, G. Nolet, G. Masters, F. A. Dahlen, and S.-H. Hung. Global P and PP traveltime tomography: rays versus waves. *Geophys. J. Int.*, 158:637–654, 2004.

[34] S. Osher and R. P. Fedkiw. *Level Set Methods and Dynamic Implicit Surfaces*. Springer-Verlag, New York, 2003.

[35] S. Osher and J. A. Sethian. Fronts propagating with curvature dependent speed: algorithms based on Hamilton-Jacobi formulations. *J. Comput. Phys.*, 79:12–49, 1988.

[36] D.N. Ostrov. Extending viscosity solutions to eikonal equations with discontinuous spatial dependence. *Nonlinear Analysis*, 42:709–736, 2000.

[37] D. Peng, B. Merriman, S. Osher, H. K. Zhao, and M. Kang. A PDE-based fast local level set method. *J. Comput. Phys.*, 155:410–438, 1999.

[38] R.E. Plessox. A review of the adjoint-state method for computing the gradient of a functional with geophysical applications. *Geophys. J. Int.*, 167:495–503, 2006.

[39] J. Qian, Y-T Zhang, and H-K. Zhao. Fast sweeping methods for eikonal equations on triangulated meshes. *SIAM J. Numer. Analy.*, 45:83–107, 2007.

[40] J. Qian, Y-T Zhang, and H-K. Zhao. Fast sweeping methods for static Hamilton-Jacobi equations triangulated meshes. *J. Sci. Comp.*, 31:237–271, 2007.

[41] N. Rawlinson, J. Hauser, and M. Sambridge. Seismic ray tracing and wavefront tracking in laterally heterogeneous media. *Adv. Geophs.*, 49:203–267, 2007.

[42] F. Santosa. A level-set approach for inverse problems involving obstacles. *Control, Optimizat. Calculus Variat.*, 1:17–33, 1996.

[43] A. Sei and W. W. Symes. Gradient calculation of the traveltime cost function without ray tracing. In *65th Ann. Internat. Mtg., Soc. Expl. Geophys., Expanded Abstracts*, pages 1351–1354. Soc. Expl. Geophys., Tulsa, OK, 1994.

[44] A. Sei and W. W. Symes. Convergent finite-difference traveltime gradient for tomography. In *66th Ann. Internat. Mtg., Soc. Expl. Geophys., Expanded Abstracts*, pages 1258–1261. Soc. Expl. Geophys., Tulsa, OK, 1995.

[45] J. A. Sethian. *Level set methods*. Cambridge Univ. Press, second edition, 1999.

[46] C. W. Shu and S. J. Osher. Efficient implementation of essentially non-oscillatory shock capturing schemes. *J. Comput. Phys.*, 77:439–471, 1988.

[47] P. Stefanov and G. Uhlmann. Rigidity for metrics with the same lengths of geodesics. *Math. Res. Lett.*, 5:83–96, 1998.

[48] P. Stefanov and G. Uhlmann. Stability estimates for the X-ray transform of tensor fields and boundary rigidity. *Duke Math. J.*, 123:445–467, 2004.

[49] P. Stefanov and G. Uhlmann. Boundary rigidity and stabiliy for generic simple metrics. *J. Am. Math. Soc.*, 18:975–1003, 2005.

[50] P. Stefanov and G. Uhlmann. Recent progress on the boundary rigidity problem. *Electron. Res. Announc. Am. Math. Soc.*, 11:64–70, 2005.

[51] P. Stefanov and G. Uhlmann. Integral geometry of tensor fields on a class of non-simple Riemannian manifolds. *Am. J. Math.*, 130:239–268, 2008.

[52] P. Stefanov and G. Uhlmann. The geodesic X-ray transform with fold caustics. *Analysis and PDE*, 5:219–260, 2012.

[53] R. Tsai, L.-T. Cheng, S. J. Osher, and H. K. Zhao. Fast sweeping method for a class of Hamilton-Jacobi equations. *SIAM J. Numer. Anal.*, 41:673–694, 2003.

[54] G. Uhlmann. Travel-time tomography. *J. Korean Math. Soc.*, 38:711–722, 2001.

[55] G. Uhlmann and S. Hansen. Recovering acoustic and elastic parameters from travel-times. In *International Mechanical Engineering Congress and Exhibition, Proceedings*, page 32149. ASME, 2002.

[56] J. Vidale. Finite-difference calculation of travel times. *Bull., Seis. Soc. Am.*, 78:2062–2076, 1988.

[57] John K. Washbourne, James W. Rector, and Kenneth P. Bube. Crosswell traveltime tomography in three dimensions. *Geophysics*, 67:853–871, 2002.

[58] H. K. Zhao. Fast sweeping method for eikonal equations. *Math. Comp.*, 74:603–627, 2005.

[59] P. Zheglova, C. Farquharson, and C. Hurich. 2D reconstruction of boundaries with level set inversion of travel times. *Geophysical J. International*, 192:688–698, 2013.